Modeling and diagnostics of the structure of rf glow discharges in Ar at 13.56 MHz

Toshiaki Makabe and Nobuhiko Nakano
Department of Electrical Engineering, Faculty of Science and Technology, Keio University, Hiyoshi, Yokohama 223, Japan

Yukio Yamaguchi
Research Center, Mitsubishi Kasei Corporation, 1000 Kamoshida, Yokohama 227, Japan
(Received 6 May 1991)

The structure of rf glow discharges in Ar at 13.56 MHz is described, making use of a relaxation continuum model. The model includes consideration of the relaxation kinetics for the momentum and energy of charged particles. The discharge structure and plasma property are modeled using molecular quantities (i.e., collision cross sections, radiative lifetimes, etc.) and macroscopic transport quantities for charged particles. Spatiotemporal distributions for the field and the net production rate and density of particles are studied in detail in the bulk plasma as well as the ion sheath under periodic steady-state conditions. In particular, the temporal profiles including phase shift and nonlinear variation with respect to the applied-voltage wave form are discussed. Each type of excited atom shows a different spatiotemporal density distribution due to different loss mechanisms, although the production profiles are similar. That is, $Ar(^3p_5)$ is controlled by a radiative decay and quenching in collisions with $Ar(^1S_0)$, while $Ar(^3P_{0,2})$ is controlled by diffusion. The validity of the relaxation continuum model is investigated by the observation of external electric properties and the measurement of spatiotemporally resolved optical emission from the rf glow. Quantitative comparison of the results from theory and experiment supports the validity of the relaxation continuum model. The relaxation continuum model is simple and physically reasonable.

PACS number(s): 52.80.Hc, 52.25.Fi, 52.70.Kz

I. INTRODUCTION

Radio-frequency glow discharges have been used routinely in the microelectronic device fabrication and in the manufacture of new materials [1,2]. This is mainly due to their usefulness as sources of radicals and ions, which play a major role in surface reactions in plasma chemical vapor deposition (PCVD) and plasma etching. In order to optimize the performance of the processing plasma systems, detailed knowledge of the radical transport as well as of the electronic property is highly desired for rf glow discharges. For electron transport, electron heating by the high-field oscillating sheath in an rf discharge is of greater importance than the energy transfer in the bulk plasma, although the sheath dynamics cannot be considered independent of the bulk plasma properties. From the viewpoint of electron kinetics [3], the energy response of the electrons is a notable characteristic of an rf glow discharge. Investigation of a rare-gas rf discharge will lead to a better understanding of the discharge structure in advance of the development of new plasma processes. Here we study the electrical properties and the density profiles of the excited atoms in rare-gas discharges without complicated chemical processes. Rare gases such as He and Ar play an important role in the maintenance of glow discharges because of their high efficiencies in heat transfer from the bulk of the discharge to the outside, and their ability to keep the average electron energy higher. He and Ar are therefore used as buffer gases in discharges with more complicated heavy molecules. Realistic models are possible because of the work devoted to measuring both the microscopic collision cross sections between the charged particle and Ar [4–12], and the macroscopic swarm parameters in Ar [4,13–24]. Reliable radiative lifetimes and deactivation rate constants for the excited states in Ar have been also reported [25–35].

In the present work we have simulated rf glow discharges in Ar at 13.56 MHz in order to investigate the physics of a collision-dominated plasma. In preceding papers [36–38], we reported the diagnostics of rf discharges at 13.56 MHz using space- and time-resolved optical-emission spectroscopy.

High-frequency gas discharges were studied in the 1940s. The primary mechanisms governing the high-frequency breakdown and the steady-state microwave plasma are qualitatively understood [39–41]. Nevertheless, the quantitative understanding of the discharge is weak because of the lack of the microscopic physical and chemical quantities and the difficulty of theoretical treatments of the time dependence of the charged-particle transport.

In an rf glow discharge, there are two distinct regions, each with different charged-particle transport. They are the bulk plasma and the ion sheath, which are closely coupled with each other. A self-consistent continuum theory is highly desired in modeling both dc and rf discharges in order to overcome the limits of classical theories applied to the sheath and the bulk plasma, respectively [42–45]. The historical development of the modeling of dc glow discharges has been reviewed [46–49]. The industrial angular frequency ω (i.e., 13.56

MHz) is generally in the range $\omega_{pi} < \omega < \omega_{pe}$, where ω_{pi} and ω_{pe} are, respectively, the macroscopic plasma frequencies for ions and electrons as defined in a collisionless plasma [50]. The frequency is also in the range $t_i \gg \omega^{-1} \geq t_e$, where t_e and t_i are the transit times between electrodes of electrons and ions in a collision-dominated plasma, respectively. Under these circumstances, the discharge is principally maintained by volume ionization without the need for secondary-electron emission by ions at the electrodes. The electrode sheath is mainly capacitive, i.e., the displacement current is dominant compared with the conduction current in the sheath.

During the past few years, rapid advances in the quantitative understanding of rf glow discharges have been achieved using simulations based on fluid theory [53–57, 60, 62–68] and particle models [51, 52, 58, 59, 69–71]. Fluid-theory models can be classified into groups based on the local-field approximation [54,57,62,63], the quasi-thermal approximation [53,56,65–68], and the relaxation continuum model [60,64]. Particle-in-cell and/or Monte Carlo simulations are particle models [51,52,59,69–71]. Recently, rf glow discharges in He were studied using a phase-space analysis of the Boltzmann equation by Sommerer, Hitchon, and Lawler [61]. Much of the modeling in Ar at 13.56 MHz has been presented (Table I) [54–56, 66]. Fundamental interest in Ar at about 0.1–1 Torr is motivated by a need to understand the physical kinetics in the discharge involving the ions heavier than H^+ or He^+.

This paper describes a systematic study of capacitively coupled rf glow discharges in Ar. We assume that the electrodes are planar and large enough to neglect their sheath edge areas. The discharge will thus be considered one dimensional. The area of interest is the collision-dominated, low-gas-temperature discharge with the spatiotemporal modulation of both the bulk plasma and the sheath. Under these circumstances, the local electron-energy balance is disturbed. That is, the electron transport has finite delays with respect to the local instantaneous reduced field $E(z,t)/N$ [3,72–76]. This is caused by the lack of collisional energy and/or momentum relaxation between the electron and the molecule within the characteristic time or distance. In a previous paper, the relaxation continuum model was briefly mentioned, and an analysis was conducted on the influence of the applied frequency in an rf discharge [60]. The basic principle of the model is to represent the system in a relatively simple yet physically reasonable manner.

One of the purposes of this paper is to present an expression for the nonhydrodynamic effect in an rf glow discharge by the relaxation continuum model. The

TABLE I. rf glow discharge properties at 13.56 MHz in Ar, simulated by various fluid models.

	Present				Ref. [55]	Ref. [56]	Ref. [54]	Ref. [66]
f (frequency) (MHz)	13.56				13.56	13.56	13.56	13.56
p (pressure) (Torr)	1.0	1.0	0.5	0.1	0.5	0.8	0.3	0.8
V_0 (amplitude) (V)	50	100	120	160	347	14	270	50
J_0 (amplitude) (mA cm^{-2})	0.83	2.19	2.72	3.04	3.9	0.6	12.7	1.0
d (electrode distance) (cm)	2.0				2.0	3.5	5.0	2.0
T_g (gas temperature) (K)	273					273		300
γ (secondary coefficient)	0.01					0.05		
W (mean power) (mW cm^{-2})	8.4	33.3	33.3	33.3	0.07	1.0		
ϕ (phase shift) (deg)	66.6	72.0	78.5	81.4	84	76	68.3	
Ni_{max}, Ne_{max} (10^9 cm^{-3})	1.82	3.44	3.52	10.3	6.8	16.0	60.0	7.0
Shape of $N_i(t)$ $N_i(z)$	Time-independent Single maximum				Time-independent Single maximum	Time-independent Single maximum	Double maxima	Time-independent Single maximum
Plasma potential, V_p	$V_p > V_{ground}$ $V_p > V_{rf}$				$V_p > V_{ground}$ $V_p > V_{rf}$			$V_p > V_{ground}$ $V_p > V_{rf}$
Maximum sheath width (cm)	Always present					Always present		Always present
	0.27	0.24	0.28	0.30	0.4–0.5			0.26
Maximum field (Vcm^{-1})								
in sheath	425	830	1008	1100				
in bulk center	11.7	12.5	8.0	0.6				

theory is based on the numerical solution of Poisson's equation in conjunction with the continuity equation for electrons and ions by considering the momentum and energy relaxations due to collisions. The validity of the relaxation continuum model is then investigated by the use of space- and time-resolved optical diagnostics of the rf glow discharge at 13.56 MHz in Ar. A detailed comparison between the previous and present results is made for the electrical properties and the spatiotemporal profiles of the net excitation rate and the density distributions of excited atoms.

II. DESCRIPTION OF THE RELAXATION CONTINUUM MODEL

A. Description of the model

A parallel-plate rf discharge is considered, maintained by an applied voltage with angular frequency ω,

$$V(t)=V_0\cos\omega t \ . \tag{1}$$

The discharge has a spatiotemporal structure consisting of both the sheaths in front of the electrodes and of the bulk plasma. The inner field varies strongly in time and space. It is therefore essential to have an expression for the nonhydrodynamic phenomena having time- and space-dependent swarm parameters [77]. The system is described in one-dimensional position space by the relaxation continuum model. The model is based on the equations governing the density, the average velocity, and the effective field of the charged particles by considering the relaxation kinetics. These equations are derived from the velocity moments of the Boltzmann equation [78], and written as

$$\frac{\partial g(\mathbf{v},z,t)}{\partial t}+\mathbf{v}\cdot\nabla_z g(\mathbf{v},z,t)+\frac{e\mathbf{E}(z,t)}{m}\cdot\nabla_v g(\mathbf{v},z,t)=J(g) \ , \tag{2}$$

where $g(\mathbf{v},r,t)$ is the velocity distribution function for the electron or ion. e and m are, respectively, the charge and mass of the electron or ion. Further, $\mathbf{v}$, z, and t denote the velocity, axial position, and time, respectively, while J is the collision term. $E(z,t)$ is the local instantaneous electric field. The continuity equation for the electron and ion is then written by the zero-order velocity moment of Eq. (2) as

$$\frac{\partial n_j(z,t)}{\partial t}+\frac{\partial[n_j(z,t)v_j(z,t)]}{\partial z}=R_i(z,t)n_e(z,t) \ , \tag{3}$$

where $n_e(z,t)$ is the electron number density, and $R_i(z,t)$ is the ionization rate. $v_j(z,t)$ is the average velocity of the electron or ion, usually given by the sum of the drift and diffusion velocities as

$$v_j(z,t)=v_{dj}(z,t)+v_{Dj}(z,t) \ . \tag{4}$$

The two-step ionization from the excited atom and the volume recombination are neglected under the conditions for a weakly ionized gas. The momentum-transfer equation given by the first-order moment of the Boltzmann equation can be described as a form of the relaxation equation,

$$\frac{\partial[m_j v_j(z,t)]}{\partial t}=eE(z,t)-\frac{m_j v_j(z,t)}{\langle\tau_m\rangle}-\frac{m_j v_j(z,t)\partial v_j(z,t)}{\partial z} \ . \tag{5}$$

The momentum relaxation time $\langle\tau_m\rangle$ is given by $m_j v_j(z,t)/eE$, making use of the dc value of the average speed as a function of E/N. The second moment of the Boltzmann equation yields, in principle, the conservation of energy. Under nonequilibrium conditions, the conservation of the mean electron energy $\varepsilon_{me}(z,t)$ will be given in a straightforward manner by considering the energy gain from the field and the collisional energy loss [78] as

$$\frac{\partial[\varepsilon_{me}(z,t)n_e(z,t)]}{\partial t}=eE(z,t)n_e(z,t)v_e(z,t)-\left[(2m/M)R_m\varepsilon_{me}(z,t)+\sum_{R,\varepsilon}R_{\rm ex}\varepsilon_{\rm ex}+R_i\varepsilon_i\right]n_e(z,t)-\frac{\partial[n_e(z,t)v_e(z,t)\varepsilon_{me}(z,t)]}{\partial z} \ , \tag{6}$$

where m/M is the electron-molecule mass ratio. R_m, $R_{\rm ex}$, and R_i are, respectively, the rates of the elastic momentum transfer, excitation, and ionization, and $\varepsilon_{\rm ex}$ and ε_i are the threshold energies of the excitation and ionization. Here, the effective field for $\varepsilon_{me}(z,t)$ is defined by $E_{\rm eff}^2=\varepsilon_{me}/e\mu\langle\tau_e\rangle$, with μ the electron mobility. Then, $E_{\rm eff}^2$ satisfies the relaxation equation,

$$\frac{\partial[E_{\rm eff}(z,t)^2n_e(z,t)]}{\partial t}=-[E_{\rm eff}(z,t)^2-E(z,t)^2]\frac{n_e(z,t)}{\langle\tau_e\rangle}-\frac{\partial[v_e(z,t)n_e(z,t)E_{\rm eff}(z,t)^2]}{\partial z} \ . \tag{7}$$

Here, $\langle\tau_e\rangle$ represents the energy relaxation time for the average electron energy, and is related to the collisional energy-loss rate for a collision-dominated discharge as

$$\langle\tau_e\rangle^{-1}=(2m/M)R_m+\left[\sum_{R,\varepsilon}R_{\rm ex}\varepsilon_{\rm ex}+R_i\varepsilon_i\right]\Big/\varepsilon_{me} \ . \tag{8}$$

The value of $\varepsilon_{me}(z,t)$ at position z and time t is then given by the function $E_{\rm eff}(z,t)/N$ from the values already obtained under uniform and constant reduced field strength. It should be noted that the energy relaxation time depends strongly on the type of collision. $\langle\tau_e\rangle$ for an inelastic collision is usually less than 10^{-8} s at 1 Torr, while the time for elastic scattering has a magnitude of 10^{-6} s [76]. The difference in the relaxation time has a great

influence on the values of the swarm parameters [3,75,76]. It is therefore necessary to have an implicit procedure with the initial value of $\langle \tau_e \rangle$ *a priori,* except when $\langle \tau_e \rangle$ is constant. The time constants for the excitation and ionization rates are assigned to different values of $\langle \tau_{ej} \rangle$ and $\langle \tau_{ei} \rangle$, respectively, by the same concept as in Eq. (8). That is, the effective fields defined by the relaxation of average energy are used in order to determine excitation and ionization rates, etc. from quasiequilibrium drift-tube data. In Eqs. (3), (5), and (7) the local instantaneous field $E(z,t)$ is related to the electron and ion densities by Poisson's equation,

$$\frac{\partial E(z,t)}{\partial z} = \frac{e[n_i(z,t) - n_e(z,t)]}{\epsilon_0} , \tag{9}$$

where ϵ_0 is the permittivity. It is known from swarm studies that the transport quantities have a finite delay with respect to the local instantaneous field at 13.56 MHz in collision-dominated regions [3,74–76].

Various kinds of excited species are generated in an rf glow discharge. The time and space distribution of the excited species is determined by the diffusion equation, assuming a direct excitation of the ground-state atom by electron impact, as

$$\frac{\partial n^*(z,t)}{\partial t} = D^* \frac{\partial^2 n^*(z,t)}{\partial z^2} + R_{ex}(z,t) n_e(z,t) - \frac{n^*(z,t)}{\tau_r} - k_q n^*(z,t) N - k_{qe} n^*(z,t) n_e(z,t) , \tag{10}$$

where $n^*(z,t)$ is the number density. D^* and τ_r are the diffusion coefficient and the radiative lifetime of the excited atom, respectively, k_q and k_{qe} denote the quenching rates of the excited atom by a ground-state atom and an electron, respectively.

B. Boundary conditions and swarm parameters

Perfectly absorbing metallic electrodes are assumed. The boundary conditions for the charged particles are the density balances. That is, the boundary conditions are written as $n_e = n_i = 0$, and $E_{\text{eff}} = 0$ at the ground ($z = 0$) and at the rf ($z = d$) electrodes. The secondary-electron currents at both electrodes are considered to be given by

$$j_e(0,t) = \gamma j_i(0,t) \tag{11a}$$

and

$$j_e(d,t) = \gamma j_i(d,t) . \tag{11b}$$

Here, j_e and j_i are the electron and ion currents, respectively, just in front of the electrodes, and γ is the secondary ionization coefficient for the ion. The ejection of electrons is not taken into account for the excited atoms and the photons at the electrodes. Also, n^* is set to zero at $z = 0$ and d. In this study, the numerical outer conditions are coincident with the experimental system in order to check the validity of the model. The electrode distance d is fixed at 2 cm. The gas temperature is 300 K and γ is set to 0.01 [79]. The amplitudes of the applied voltage are, respectively, 50 and 100 V at 1 Torr, and 120 and 160 V for 0.5 and 0.1 Torr, at 13.56 MHz (see Table I).

The transport coefficients for the charged particles in an rf field, under local nonequilibrium conditions, are derived from the concept of E_{eff}/N using the values under uniform and constant reduced field strength as mentioned above. The original quasiequilibrium data can be found in the literature. Values for $\mathbf{v}_{de}$ and D_{Le} are taken from the work of Kucukarpaci and Lucas [22]. We refer to the data of Ellis *et al.* [80] for $\mathbf{v}_{di}$ and Sejkora *et al.* [81] and Dall'Armi *et al.* [82] for D_{Li}. The value of R_i for Ar with the ionization energy of 15.6 eV was obtained by multiplying the ionization coefficient (Dutton [17]) by the electron drift velocity. The transport quantities of the excited species in Ar are listed in Table II. In particular, the excitation frequency R_{ex} for Ar($^3P_{0,2}$), Ar($^2p_1$), and Ar($^3p_5$), having excitation energies of 11.5, 13.48, and 14.57 eV, respectively, is taken from the experimental values of Tachibana [16] by multiplying $\mathbf{v}_{de}$.

C. Numerical procedure

The manner of obtaining the initial conditions for a periodic steady-state rf glow discharge is as follows. It is possible to choose *a priori,* spatiotemporal density profiles of both the electrons and ions as the initial distributions, in order to save computation time. In the present work, the initial conditions n_e and n_i are taken to be

$$n_e(z,t) = n_0 \sin(\pi z/d) , \tag{12a}$$

$$n_i(z,t) = n_0 \sin(\pi z/d) , \tag{12b}$$

together with the initial field distribution, $E(z,t) = 0$.

The numerical technique used to solve the system of equations is as follows. Space and time are, respectively, divided into 51 and 400–4000 steps. For each time step, the quantities in the rf glow discharge are iteratively solved over the entire space domain by the Newton-Raphson method, with the time derivatives of the system represented by the sixth-order Gear's algorithm [83]. This procedure is repeated, starting from a given set of appropriate initial conditions, until a harmonic steady state is obtained for the quantities.

III. RESULTS AND DISCUSSION

A. Electrical properties of the rf glow discharge in Ar

An overview of the rf glow discharge field in Ar at 13.56 MHz, $V_0 = 50$ V, and 1 Torr is shown in Fig. 1 in the form of the space-time distribution, $E(z,t)$. The spatial distribution at $\omega t = 0$ has an inclination similar to a dc discharge with the cathode at $d = 0$; that is, a strong and steep-gradient field develops in front of the grounded electrode. This region is known as the ion sheath. The rf glow discharge is characterized by the oscillating high-field sheath with time in front of both electrodes. The sheath fields are mostly linear and usually exist more or less in front of electrodes with opposite polarities during a period. As a result, the field acts on the electrons,

confining them to the bulk plasma between the two sheaths. This indicates the presence of a continual positive plasma potential in the bulk during a period. That is, the plasma potential temporally varies from a maximum of 69 V to a minimum of 20 V at the center. In greater detail, the maximum field occurs at 4.6 ns ($\omega t = 0.125\pi$) after the peak of the applied voltage wave form. This indicates the beginning of the collapse of an electron transit between electrodes during a half period, as well as for an ion at 13.56 MHz. At the anodic part of the polarity, the electron current is controlled by diffusion, since the density gradient is very steep in the vicinity of the electrode. The sheath width is defined as the distance from the electrode to the crossing point between the asymptotic lines of the sheath and bulk fields. Although the field in the bulk plasma is roughly estimated to be constant and very weak, the enlarged Fig. 1(b) shows the presence of a time varying sinusoidal field with a frequency of ω and a large phase shift as compared with the wave form in the sheath. The field at the center of the bulk plasma has the form

$$E(d/2,t) = 12\cos(\omega t - 0.65\pi) \ . \tag{13}$$

TABLE II. Microscopic and transport quantities of excited atoms and ions (upper) and simulated net production rates and densities of species at 13.56 MHz in Ar. Dashes denote no consideration or independence.

	$Ar(^3P_{0,2};1s_{3,5})$	$Ar(2p_1)$	$Ar(^3p_5)$	Ar^+
Threshold energy (eV)	11.72, 11.55	13.48	14.57	15.76
Production rate	$R_j/N(E_{eff}/N)$[a]	$R_j/N(E_{eff}/N)$[a]	$R_j/N(E_{eff}/N)$[a]	$R_i/N(E_{eff}/N)$[b]
Diffusion coefficient ($10^{18}\,cm^{-1}s^{-1}$)	1.8[c], 1.8[c]	1.8	1.8	$D_L/N(E_{eff}/N)$[d]
Radiative lifetime (10^{-9} s)	$>1.3\times10^{9}$[e]	21[f]	95[g]	---
Two-body self-quenching rate ($10^{-15}\,cm^3s^{-1}$)	5.3[c], 2.1[c]	$\sim5\times10^4$	3.5×10^{5}[h]	---
Three-body self-quenching rate ($10^{-32}\,cm^6s^{-1}$)	0.83[c], 1.1[c]	---	---	---
Deactivation rate by electron ($10^{-7}cm^3s^{-1}$)	2.1[i], 1.5[i]	---	---	---
$\Lambda(z,t)_{max}$ ($10^{12}\,s^{-1}$)				
(space, time) (mm, ns)	3.54×10^2	7.10×10	2.20	2.52×10^3
1.0 (Torr)	(2.60, 65.6)	(2.23, 63.6)	(2.40, 64.5)	(2.00, 64.5)
50 (V)	(17.4, 28.8)	(17.8, 26.7)	(17.6, 28.7)	(18.0, 27.6)
	1.15×10^3	2.37×10^2	7.50	1.02×10^4
1.0 (Torr)	(2.19, 62.9)	(1.62, 61.6)	(1.62, 61.5)	(1.62, 59.4)
100 (V)	(17.8, 26.0)	(18.4, 24.7)	(18.4, 24.6)	(18.4, 22.5)
	9.82×10^2	2.35×10^2	7.23	1.27×10^4
0.5 (Torr)	(2.86, 63.1)	(2.46, 59.7)	(2.46, 59.6)	(2.19, 59.4)
120 (V)	(17.1, 26.2)	(17.5, 22.8)	(17.5, 22.7)	(17.8, 22.5)
	4.7×10^2	1.9×10^2	6.1	1.3×10^4
0.1 (Torr)	(4.09, 71.0)	(3.91, 67.2)	(3.65, 67.0)	(3.48, 66.0)
160 (V)	(15.9, 34.1)	(16.1, 30.3)	(16.4, 30.0)	(16.5, 29.1)
n_{max} (cm^{-3})				
(space, time) (mm, ns)	---	7.97×10^5	3.60×10^4	1.82×10^9
1.0 (Torr)		(2.30, 0)	(2.15, 2.76)	(1.0, ---)
50 (V)		(17.7, 36.5)	(17.8, 39.6)	
	1.50×10^{11}	2.60×10^6	1.26×10^5	3.44×10^9
1.0 (Torr)	(1.0, ---)	(2.01, 70.6)	(2.01, 73.1)	(1.0, ---)
100 (V)		(18.0, 33.7)	(18.0, 36.2)	
	1.50×10^{11}	2.58×10^6	1.57×10^5	3.53×10^9
0.5 (Torr)	(1.0, ---)	(2.63, 70.1)	(2.59, 72.7)	(1.0, ---)
120 (V)		(17.4, 33.2)	(17.4, 35.8)	
	1.49×10^{11}	2.16×10^6	1.65×10^5	1.02×10^{10}
0.1 (Torr)	(1.0, ---)	(3.86, 2.43)	(3.86 4.13)	(1.0, ---)
160 (V)		(16.1, 39.3)	(16.1, 41.0)	
Control mechanism	Diffusion	Lifetime	Self-quenching	Diffusion

[a]Reference [16].
[b]Reference [17].
[c]Reference [90].
[d]Reference [82].
[e]Reference [91].
[f]Reference [31].
[g]Reference [33].
[h]Reference [37].
[i]Reference [92].

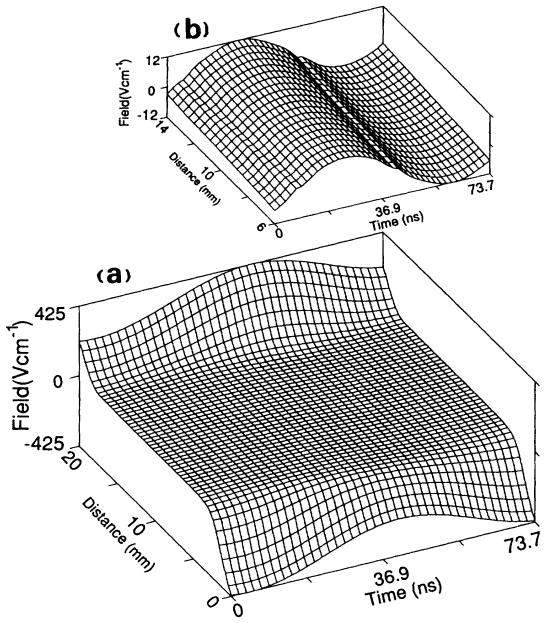

FIG. 1. (a) Spatiotemporal field distribution of the rf glow discharge in Ar for $f=13.56$ MHz, $V_0=50$ V, and $p=1$ Torr. (b) An enlarged figure of the bulk plasma.

This exhibits a weak penetration of the driving rf field into the bulk plasma. The appearance of the large phase shift in the bulk field compared with the sheath was also found in He at 13.56 MHz and 0.1 Torr by Sommerer, Hitchon, and Lawler [61]. The phase shift arises both from the requirement of the spatial conservation of total current and from the difference in current components between the sheath and the bulk plasma. Although the spatial components of the total current will be discussed later in Fig. 3, it is important to point out that the current in the sheath is mostly comprised of the displacement current J_D, with the peak appearing at t_m in the maximum of $\partial E(z,t)/\partial t$, not in $E(z,t)$. As a result, the bulk field has to be maximum at the same time, t_m, to carry the maximum current by electron drift flow. The unusual behavior in the vicinity of $E=0$ in Fig. 1(b) is caused by the lack of full convergence of the calculation. The ensemble average of electron energy in the bulk plasma under the conditions given in Eq. (13) is independently calculated at 5.3 eV by the direct numerical procedure using the Boltzmann equation [88]. In Table I, the electrical properties are summarized and compared with previous studies [54–56,66].

When the pressure varies from 1.0 to 0.1 Torr under a constant input power of 33.3 mW cm^{-2}, the maximum sheath width expands from 2.4 to 3.0 mm in order to compensate for the lack of net ionization in the sheath and to overcome the increased loss in the flux of charged particles toward the electrodes. The full width at half maximum (FWHM) of $n_i(z)$ for a stationary distribution occupies 97%, 96%, and 76% of the space between the electrodes at pressures of 1.0, 0.5, and 0.1 Torr, respectively. Also, the space profiles of n_e and n_i at 1 Torr have the same single maximum of 3.44×10^9 cm^{-3}, almost independent of time at the center, with their maximum density rapidly increasing as the gas pressure approaches 0.1 Torr. As a result, the amplitude of the sustaining voltage increases from 100 to 160 V, and the phase shift between the applied voltage and total current approaches $\pi/2$. Simultaneously, an increase in the maximum sheath field and a drop in the bulk field occurs (see Table I). If much power is put into the discharge, n_e and n_i result in a double-peaked profile at both sheath edges in space, owing to the excess production [54]. It will be of interest to compare the present electron densities in Table I with the experimental values in a planar discharge at 13.56 MHz found in microwave transmission spectroscopy by de Vries, van Roosmalen, and Puylaert [84]. The microwave diagnostics yield values in the range of $(2.8-3.8)\times10^9$cm^{-3} for a power density of 30 mW cm^{-2} with the aluminum electrodes. The present results show good quantitative agreement with the measurements.

The formation of a double layer in front of the instantaneous anode in electronegative gases in low [57,85] and high frequency [38,64] glow discharges has been pointed out in both experiment and theory. With an electropositive heavier gas, Ar, the double layer is not formed at 13.56 MHz, as shown in Fig. 1. However, in an electropositive gas, the double-layer formation may be realized by the lack of ions in front of the instantaneous anode, since the ion density with a light mass will be reduced in this region. Experimental evidence has recently been obtained for H_2 at 13.56 MHz [86].

Figure 2 shows the applied voltage, total current, and dissipated power characteristics during one period at 1 Torr and $V_0=100$ V. The current has a sinusoidal wave form under these outer discharge conditions. The current wave form leads the applied voltage by 72.0°. The discharge is then termed as capacitive. The power density, calculated by $V(t)J(t)$, has positive values except over the ranges $0.1\pi<\omega t<0.5\pi$ and $1.1\pi<\omega t<1.5\pi$. The time-averaged power density of 33.3 mW cm^{-2} is dissipated in the discharge. The appearance of the sinusoidal nature in the total current depends on the percentage of the displacement current at the sheath; that

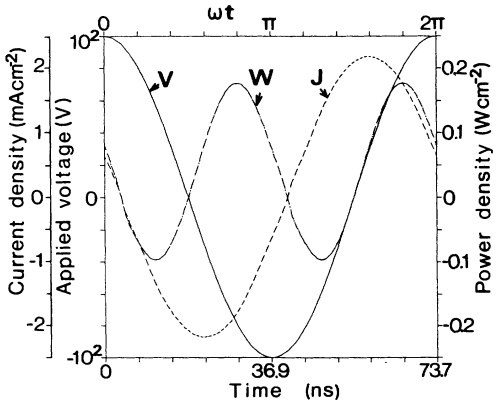

FIG. 2. Total current, applied voltage, and dissipated power characteristics in Ar for $f=13.56$ MHz, $V_0=100$ V, and $p=1$ Torr.

is, the total current density consists of conduction components of electrons and ions, j_e and j_i, and of the displacement current j_D. The displacement current density can be expressed in terms of the density of the charged particle as

$$j_D(z,t)=e\partial\int_z^{z+dz}[n_i(z,t)-n_e(z,t)]dz/\partial t\ . \qquad (14)$$

When the ion transit time between electrodes t_i is much larger than ω^{-1}, the drift motion of the ion is trapped. In this case, the spatial density of the ions is almost independent of the phase during the period of the applied voltage, i.e., $\partial n_i/\partial t\sim 0$. This corresponds to the present case. Therefore, if the time derivative of $n_e(z,t)$ has a sinusoidal wave form, the displacement current given by Eq. (14) will exhibit a sine wave. These features can be understood from the position dependence of each component of the current densities at four different phases during the first half period, under conditions of 1 Torr and $V_0=100$ V shown in Fig. 3. The current profile in the succeeding second half period is obtained by changing the sign and the z direction displayed in Fig. 3. The sign of the current density is taken to be positive when electrons flow along the z axis. There is a slight influence of ion diffusion in front of the electrodes. The dominant current components are the electron in the bulk plasma and the displacement current in the sheath, since the physical relations $\omega_{pi}\ll\omega<\omega_{pe}$ and $t_i\gg\omega^{-1}\geq t_e$ are fulfilled. The electron current in the sheath in front of the grounded electrode over the range $0.25\ \pi<\omega t<\pi$ mainly results from diffusion opposite the drift direction due to the large gradient of n_e. Similar flow occurs in front of the rf electrode during the remaining portion of the period. The electrons in the bulk at 1 Torr are always transported by electron drift under the time-varying fields [see Fig. 1(b)]. One the other hand, the ions migrate by the ambipolar diffusion in the bulk [53,78]. No abrupt change in the space distribution of each current component is found for each rf phase in Ar.

Figure 4 shows the spatiotemporal behavior of the net ionization rate $\Lambda_i(z,t)$, given by $n_e(z,t)R_i(z,t)$, between both electrodes during the period of the applied voltage under the same discharge conditions as in Fig. 1. The bulk properties are enlarged in order to investigate the electron kinetics in the bulk plasma. The generation of electrons in the sheaths is nearly zero at $\omega t=0.125\pi$ and 1.125π, when the sheath width is near its maximum and the highest sheath field is formed in front of the electrodes (see Fig. 1). This means that there is a lack of secondary-electron emission on the electrodes by the impact, since most of the ions are spatially trapped with regard to the drift motion of the applied rf frequency. Two isolated symmetric peaks, both on the order of 10^{15} $cm^{-3}s^{-1}$, appear in the net ionization rate at 1 Torr and $V_0=50$ V. The maximum arises, having a slight delay of 1 ns with respect to the current peak. The delay is intrinsic, based on the energy relaxation time for the ionization $\langle\tau_{ei}\rangle$. The sheath expansion speed is estimated from the space-time behavior of the net ionization rate as 4.1×10^6 $cm\,s^{-1}$. As a result, the discharge is maintained through the sheath volume ionization due to the reflection of electrons in front of the electrodes. In other words, the sheath expansion is the dominant electron heating mechanism [52,61,87]. In the bulk plasma, the net ionization rate $\Lambda_i(z,t)$ mainly consists of dc and even harmonics of 2ω and 4ω [3,75,76]. The temporal profile having two peaks in $\Lambda_i(z,t)$ during a period results from the periodic variation of the bulk field distribution in Fig. 1(b). It should be noted that the periodic steady-state energy distribution $f(\varepsilon,t)$ in the bulk shows a large phase shift with respect to the applied field. A recent study by Surendra, Graves, and Morey [69] using a He-like gas shows these features through a particle-in-cell Monte Carlo simulation. The nonlinear time modulation of $\Lambda_i(z,t)$ is caused

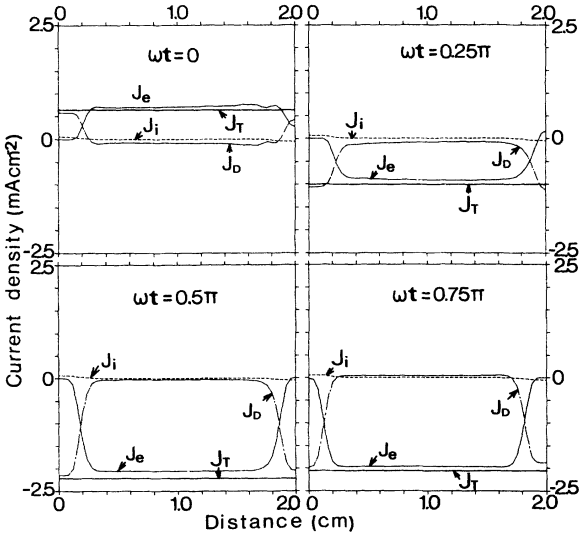

FIG. 3. Current-component distributions as a function of position for four phases of ωt. J_T, J_e, J_i, and J_D represent the total, electron, ion, and displacement current densities, respectively. The conditions are the same as in Fig. 2.

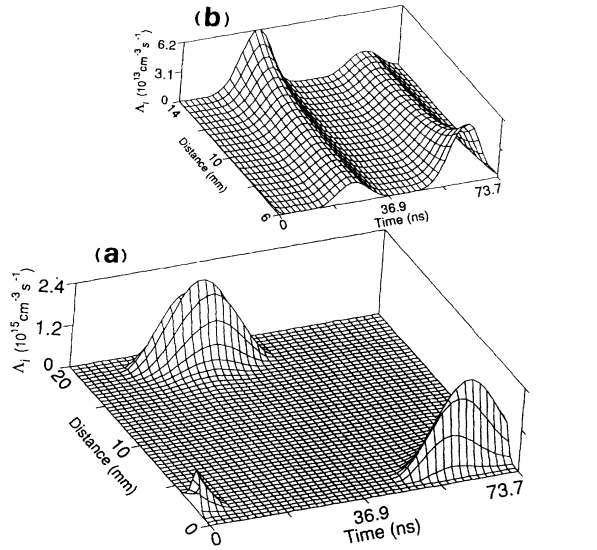

FIG. 4. (a) Spatiotemporal net ionization rate $\Lambda_i(z,t)$ for the rf glow discharge in Ar; (b) is enlarged in the bulk plasma. The conditions are the same as in Fig. 1.

by the rapid attenuation of high-energy electrons with $\varepsilon > \varepsilon_i$ in $f(\varepsilon,t)$. This occurs under the condition of a low bulk field in the form of a first harmonic at 13.56 MHz [see Fig. 1(b) and Eq. (13)] [76], since the bulk density of the electrons is temporally constant. The situation in $\Lambda_i(z,t)$ at 0.1 Torr is somewhat different from 1.0 and 0.5 Torr [see Fig. 5(a)]; that is, the curve in $\Lambda_i(z,t)$ penetrates deeply into the bulk, exhibiting an exponential decay. This is directly attributable to the order of difference in the energy relaxation time between 0.1 and 1.0 Torr. Figure 5(b) shows the absolute value of the effective field distribution related to the ionization rate $R_i(z,t)$ shown in Fig. 5(a). The essential difference in the spatiotemporal profile of $E_{\text{eff}}(z,t)$ to $E(z,t)$ is that the peak position of the former is apart from the electrode surface. This is caused by the absence of electrons with energy greater than ε_i just in front of the electrode.

Under steady-state conditions, the electrons and ions in the central part of the bulk plasma maintain constant densities. Under these circumstances, the electron transport within the bulk will be investigated by the Boltzmann equation under a spatially homogeneous and a temporally varying rf field. A limited number of similar investigations have previously been carried out [3,72,74–76]. In particular, the nonlinear energy response of the instantaneous energy distribution has recently been reported both by the expansion method and by the direct numerical procedure of the velocity distribution [88].

B. Properties of excited species of the rf glow discharge in Ar

The net production rate of excited atoms $\Lambda_j(z,t)$ is investigated for three different energy levels, $^3P_{0,2}$, $^2p_1$, and $^3p_5$ in Ar. The $\Lambda_j(z,t)$ for the metastable state, Ar ($^3P_{0,2}$), at 1 Torr and $V_0=50$ V, is shown in Fig. 6. The appearance of two symmetric peaks in $\Lambda_j(z,t)$ during a period is similar to those in the net ionization rate; however, the time and space dependence differs slightly (see Table II). It is found that the peak more closely approaches the electrode in space and becomes faster in time when the threshold energy of the formation process is increased. The magnitude depends on the shape of the excitation cross section between the electron and the atom. Experimental evidence of the relationship between the peak position and the threshold energy has recently been reported for the rf discharge in CH_4-H_2 mixtures [36] and Ar [37] by the use of spatiotemporally resolved optical-emission spectroscopy.

The length from the peak of the emission intensity to the nearest electrode is measured as the sheath width in some experimental work [89]. Attention will be focused on the fact that the sheath width determined by the emission peak differs in detail between the target lines.

The production of excited atoms is noticeable, even in the bulk plasma compared with the ionization due to the relation $\varepsilon_j < \varepsilon_i$. No rate is found in the vicinity of both electrodes due to the lack of electrons, although the high field is always maintained in front of the electrodes (see Fig. 1). When the time development of $\Lambda_j(z,t)$ is estimated by the arrival time spectrum, as marked by arrows (↓) in Fig. 6, it is against the migration of electrons in the bulk plasma, although it follows the electrons at the sheath (see Fig. 3). This is due to the fact that $\Lambda_j(z,t)$ is not caused by the simple electron avalanche from the sheath to the bulk, but is composed both of the avalanche of electrons with large multiplication in the sheath and of high-density plasma electrons under a small sinusoidal field, as shown in Fig. 1(b). The estimation of the sheath expansion velocity from Fig. 6 can be made by the arrival distance spectrum denoted by the arrows (→), the velocity being 4.2×10^6 cm s^{-1}.

Excited atoms exhibit several distinctive density distri-

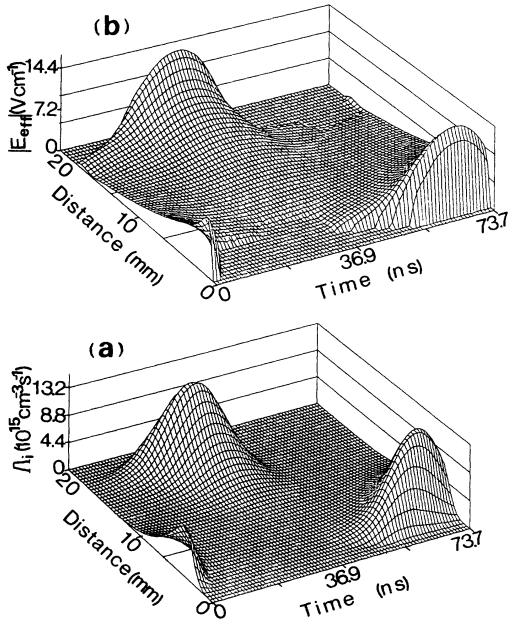

FIG. 5. Spatiotemporal distributions of the net ionization rate $\Lambda_i(z,t)$ and the related effective field $|E_{\text{eff}}(z,t)|$ in Ar for $f=13.56$ MHz, $V_0=160$ V, and $p=0.1$ Torr. (a) $\Lambda_i(z,t)$; (b) $|E_{\text{eff}}(z,t)|$.

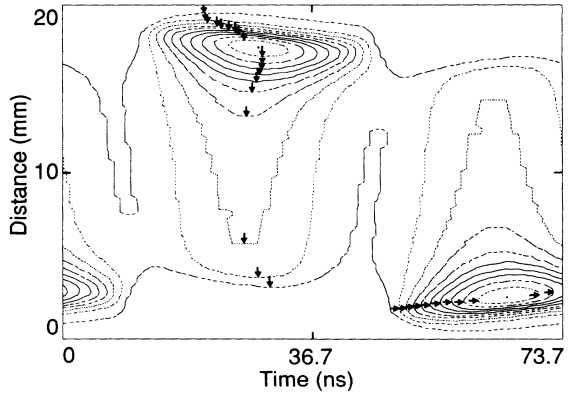

FIG. 6. Contours of the spatiotemporal net production rate $\Lambda_j(z,t)$ for the metastable state Ar($^3P_{0,2}$). The contour increment is constant, equal to 10% of the maximum value, 3.5×10^{14} cm$^{-3}s^{-1}$. Sheath expansion is denoted by the horizontal arrow →, and the arrival time spectrum is marked with a vertical arrow ↓ (see text). The conditions are the same as in Fig. 1.

butions owing to the type and magnitude of the loss mechanism, although they have a similar production profile [see Figs. 7(a) and 7(b)]. It can be found when comparing Figs. 7(a) and 7(b) that the neutral active species diffusing to the electrode is controlled by the fundamental microscopic processes. The density distribution of the metastable state, Ar ($^3P_{0,2}$) in Fig. 7(a), has a profile controlled by diffusion, independent of time, with a maximum 1.5×10^{11} cm^{-3} at the center of the space between the electrodes.

In this simulation, it is postulated that the excited species is immediately deexcited without reflection at the electrode surface, i.e., $n^*=0$ at $z=0, d$. The spatiotemporal density distribution of Ar ($^3p_5$) is shown in Fig. 7(b), which should be compared with that of Ar($^3P_{0,2}$) in Fig. 7(a). The effective lifetime of Ar($^3p_5$), estimated from $\tau_{\text{eff}}^{-1}=\tau_r^{-1}+K_qN$, is 46 ns, which is about $\frac{2}{3}$ of the period of the applied voltage and much shorter than the characteristic diffusion time of 7.2×10^{-3} s, given by $(d/\pi)^2/D^*$ [93]. As a result, the spatial profile is almost identical to the distribution of the production due to electron-impact excitation. On the other hand, the temporal feature shows a continual distribution superimposed by the exponential decay term with the lifetime of $\tau_{\text{eff}}=46$ ns on the collisional production term. With decreasing pressure, the sharp ridge in the density distribution of Ar($^3p_5$) becomes wider, extending to the bulk plasma. It was concluded that the density distribution of Ar($^3p_5$) is controlled by the self-quenching process with Ar($^1S_0$).

C. Comparison with experimental results

Diagnostic techniques have been developed for the rf glow discharge by the spatiotemporally resolved emission spectroscopy ($\Delta z=0.1$ mm, $\Delta t=0.2$ ns) of optically allowed excited species, as well as for the current-voltage characteristics [36–38]. Aluminum-plate electrodes having an 8.0-cm diameter are positioned parallel, with a spacing of 2.0 cm. The rf electrode is connected to a 13.56-MHz power supply through a capacitively-coupled matching network. The experimental detail has been previously described in Refs. [36–38]. The calibration of the detection system for an accurate measurement of the number density of an excited species is described in detail in Ref. [94].

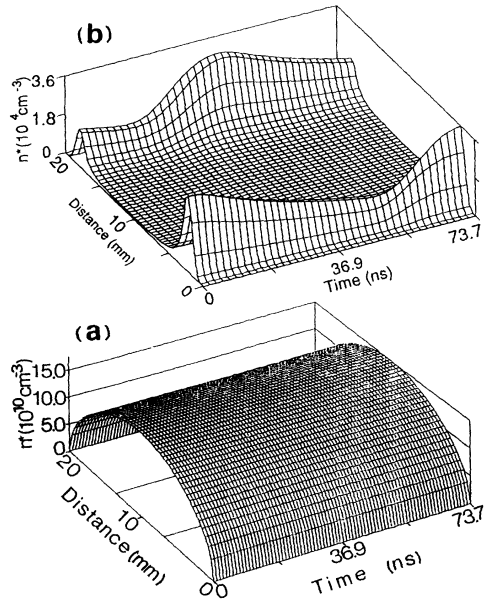

FIG. 7. Spatiotemporal density distributions for (a) Ar($^3P_{0,2}$) and (b) Ar($^3p_5$) in a periodic steady state. The conditions are the same as in Fig. 1.

In Fig. 8, showing the outer discharge parameters, a comparison is made between the theoretical and experimental values over the range, $20\le V_0\le100$ V at 1 Torr. The dissipated power is determined by $V(t)I(t)$ from the measurement of the applied voltage $V(t)$ and the total current $I(t)$ wave forms. The experimental power density is characterized by a gradual increase after a sudden rise as the amplitude of the applied voltage increases. The theoretical power density is in good agreement with the experimental power density. Recent measurements by Bletzinger [95] show reasonably good agreement with the present results for the same experimental conditions with aluminum electrodes at 14.1 MHz. The maximum sheath width exhibits a decrease with the increase in voltage amplitude. This is the physical condition required to maintain the glow discharge in front of the electrodes due to electron multiplication of reflected electrons or secondary electrons moving toward the bulk plasma. The decreasing characteristics are the direct consequence of the bulk-plasma density due to the dissipated power density. Here, the experimental width is defined as the distance between the peak of the probed emission, Ar($^3p_5\rightarrow1s_4$), and the nearest electrode. The agreement between the theoretical width and experimental width is quite good. It should be noted that even in an rf discharge at 13.56 MHz, the sheath width undergoes considerable changes due to the difference of the electrode material, as was shown in previous observations between Al and Si electrodes [37]. That is, the sheath width changes from 3 mm with Al-electrodes to 4 mm with Si under the same outer conditions, i.e., 1 Torr, $V_0=50$ V, 13.56 MHz, and 10 SCCM (SCCM denotes cubic centimeter per minute at

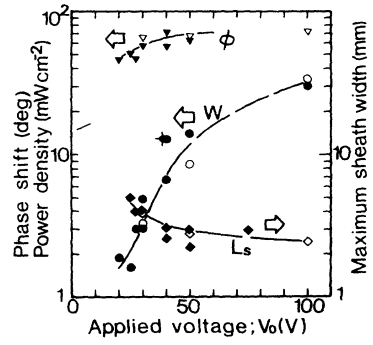

FIG. 8. Comparison of the experimental and theoretical external discharge parameters of rf glow discharges in Ar for $f=13.56$ MHz and $p=1$ Torr as a function of the amplitude of the applied voltage. ∇, ○, and ◇ denote theoretical values, while ▼, ●, and ◆ are for experimental results. -◆- ; Ref. [95].

STP). This can be explained by the difference in the secondary ionization coefficient between Al and Si, as was implied experimentally by the lack of high-energy electrons in the sheath with Si electrodes. This experimental fact suggests that high-energy electrons at the sheath, due to secondary ionization at the electrodes, play an non-negligible role in the sustaining mechanism and the structure, even for a rf discharge at 13.56 MHz. It should be noted that the phase shift between the applied voltage and total current, ϕ, increases gradually with an increase in the amplitude V_0. This can be derived from the fact that the electron diffusion flux is balanced by the drift at an earlier time in the sheath, as the electron density increases with increasing V_0.

In order to investigate the accuracy and validity of the present modeling, Fig. 7(b), which shows the density distribution of Ar($^3p_5$), should be compared with the experimental result in Fig. 9 of the time- and space-resolved optical-emission spectroscopy for the transition of Ar($^3p_5 \rightarrow 1s_4$). Both results are obtained for the same outer discharge conditions, except for the low negative dc bias voltage, -3 V in the experiment [96]. The experimental density maxima appear at 4.1 and 41 ns in time, and 3 and 17 mm in space. These values essentially agree with the theoretical values within the relative discrepancy of 2% in time and of 4% in space [see Fig. 7(b) and Table II]. The experimental maximum number density of Ar($^3p_5$) is 6.4×10^4 cm^{-3}, which is somewhat greater than the theoretical peak value of 3.6×10^4 cm^{-3}.

The spatiotemporal profile of the net excitation rate directly reflects the rf discharge structure. Comparing the net excitation rate between the experimental and theoretical distributions will yield a direct measure of the first-stage modeling using the relaxation continuum model. The spatiotemporal net excitation rate of $\Lambda_j(z,t)$ to Ar($^3p_5$) can be expeimentally obtained from the deconvolution procedure of the emission under the condition that the diffusion time of Ar($^3p_5$) from the origin is negligible when compared with the effective lifetime, $\tau_{\text{eff}}=55$ ns. Figure 10(a) shows the experimental $\Lambda_j(z,t)$ to Ar($^3p_5$), with maxima of 3.4×10^{12} cm^{-3}s^{-1} appearing at 29 and 66 ns in time, and 17 and 3 mm in space. The experimental profile can be compared with the theoretical peak values of 2.2×10^{12} cm^{-3}s^{-1} at 28.7 and 64.5 ns in time, and at 17.6 and 2.4 mm in space, shown in Fig. 10(b).

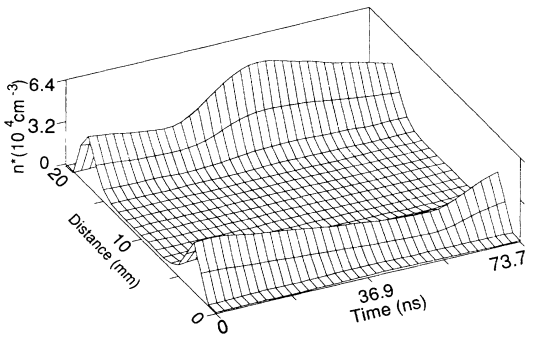

FIG. 9. Experimental spatiotemporal density distribution of Ar ($^3p_5$) in a periodic steady state. The conditions are the same as in Figs. 1 and 7 (see text).

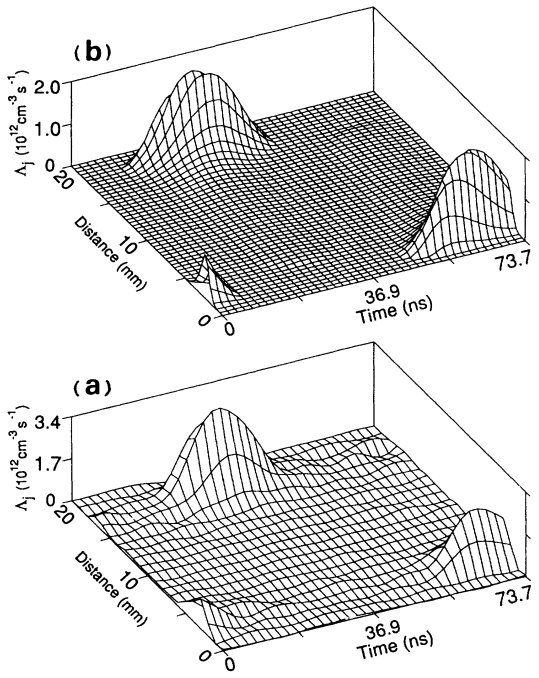

FIG. 10. Comparison of the experimental and theoretical space-time net production rate of Ar($^3p_5$). The conditions are the same as in Fig. 1. (a) Experimental; (b) theoretical.

The relative differences in time and space are, respectively, within 2% and 3% of both results. The slight disturbance and asymmetry in the field distribution between the electrodes are inherent in an experimental apparatus with a grounded metal chamber [37,96]. As a result, a divergence of the electron current will occur in front of the grounded electrode. This is the reason for the slight difference in the peak position at the side of the grounded electrode between the results. It can be concluded that the reasonable agreement between both results for the $n^*(z,t)$ and $\Lambda_j(z,t)$ of Ar($^3p_5$), as well as the electrical properties, yields experimental evidence of the validity of the present relaxation continuum model, which is simple yet physically reasonable.

IV. CONCLUSION

The modeling of an rf glow discharge has been performed by introducing the concept of the collisional relaxation time of momentum and energy for charged particles. When judging from the comparison with the experimental space-time density distribution and net excitation rate of Ar($^3p_5$) obtained from space-time-resolved optical-emission spectroscopy under the same external discharge conditions, the relaxation continuum model gave satisfactory results for the rf glow discharge structure in Ar at 13.56 MHz. The behavior of the discharge parameters, total current, dissipated power, and sheath width was also investigated as a function of the amplitude of the applied voltage. The theoretical and experimental results yielded good agreement in the low-power region, where the metastable density Ar($^3P_{0,3}$) is of minor importance to sustain the glow discharge. It was also con-

cluded that the field distribution in the bulk plasma has a phase delay of about 90° with respect to the wave form of the applied voltage. The phenomena under high-power conditions have been experimentally discussed in a previous paper [37]. The present relaxation continuum model was shown to be successful in simulating the reactive plasmas driven by a rf discharge for use in the fabrication of thin films.

ACKNOWLEDGMENTS

The authors are grateful to F. Tochikubo and S. Kakuta for helpful experimental work and valuable discussions. This work was supported by a Grant-in-Aid for Scientific Research on the Control of Reactive Plasma in Priority Areas.

[1] J. W. Coburn, R. A. Gottscho, and D. W. Hess, *Plasma Processing* (Materials Research Society, Pittsburgh, 1986).
[2] R. F. Bunshah, IEEE Trans. Plasma Sci. **18**, 846 (1990).
[3] T. Makabe and N. Goto, J. Phys. D **21**, 887 (1988).
[4] H. B. Milloy, R. W. Crompton, J. A. Rees, and A. G. Robertson, Aust. J. Phys. **30**, 61 (1977).
[5] W. C. Fon, K. A. Berrington, P. G. Burke, and A. Hibbert, J. Phys. B **16**, 307 (1983).
[6] K. L. Bell, N. S. Scott, and M. A. Lennon, J. Phys. B **17**, 4757 (1984).
[7] J. C. Nickel, K. Imre, D. F. Register, and S. Trajmar, J. Phys. B **18**, 125 (1985).
[8] J. Ferch, B. Granitza, C. Masche, and W. Raith, J. Phys. B **18**, 967 (1985).
[9] D. Rapp and P. Englander-Golden, J. Chem. Phys. **43**, 1464 (1965).
[10] K. Stephan, H. Helm, and T. D. Mark, J. Chem. Phys. **73**, 3763 (1980).
[11] P. Nagy, A. Skutlartz, and V. Schmidt, J. Phys. B **13**, 1249 (1980).
[12] E. Krishnakumar and S. K. Srivastava, J. Phys. B **21**, 1055 (1988).
[13] J. V. Bozin, V. V. Urosevic, and Z. Lj. Petrovic, Z. Phys. A **312**, 349 (1983).
[14] A. L. J. Burgmans and A. H. M. Smeets, J. Phys. D **16**, 755 (1983).
[15] C. M. Ferreira and J. Loureiro, J. Phys. D **16**, 1611 (1983).
[16] K. Tachibana, Phys. Rev. A **34**, 1007 (1987).
[17] J. Dutton, Phys. Chem. Ref. Data **4**, 577 (1975).
[18] H. B. Milloy and R. W. Crompton, Aust. J. Phys. **30**, 51 (1977); **35**, 105 (1982).
[19] A. G. Robertson, Aust. J. Phys. **30**, 39 (1977).
[20] G. L. Braglia and A. Baiocchi, Physica C **95**, 227 (1978).
[21] R. R. Abdulla, J. Dutton, and A. W. Williams, J. Phys. (Paris) Colloq. **7**, C-73 (1979).
[22] H. N. Kucukarpaci and J. Lucas, J. Phys. D **14**, 2001 (1981).
[23] T. Makabe and M. Shimoyama, J. Phys. D **19**, 2301 (1986).
[24] Y. Nakamura and M. Kurachi, J. Phys. D **21**, 718 (1988).
[25] J. Z. Klose, J. Opt. Soc. Am. **57**, 1242 (1967); **58**, 1509 (1968).
[26] T. A. Matilsky and J. E. Hesser, J. Opt. Soc. Am. **59**, 579 (1969).
[27] J. A. Kernahan, C. C. Lin, and E. H. Pinnington, J. Opt. Soc. Am. **60**, 898 (1970).
[28] G. E. Assousa, L. Brown, and W. K. Ford, Jr., J. Opt. Soc. Am. **60**, 1311 (1970).
[29] A. E. Livingston, D. J. G. Irwin, and E. H. Pinnington, J. Opt. Soc. Am. **62**, 1303 (1972).
[30] L. Minnhagen, J. Opt. Soc. Am. **63**, 1185 (1973).
[31] R. S. F. Chang and D. W. Setser, J. Chem. Phys. **69**, 3885 (1978).
[32] R. F. Firestone, T. Oka, and S. Takao, J. Chem. Phys. **70**, 123 (1979).
[33] M. J. G. Bolge and J. Campos, Physica C **119**, 359 (1983).
[34] D. Zhechev, J. Phys. B **18**, 65 (1985).
[35] H. Schmoranzer, P. Hartmetz, and D. Marger, J. Phys. B **19**, 1023 (1986).
[36] T. Kokubo, F. Tochikubo, and T. Makabe, Appl. Phys. Lett. **56**, 818 (1989).
[37] F. Tochikubo, T. Kokubo, S. Kakuta, A. Suzuki, and T. Makabe, J. Phys. D **23**, 1184 (1989).
[38] F. Tochikubo, A. Suzuki, S. Kakuta, Y. Terazono, and T. Makabe, J. Appl. Phys. **68**, 5532 (1990).
[39] H. Margenau, Phys. Rev. **73**, 297 (1948); H. Margenau and L. M. Hartman, *ibid.* **73**, 309 (1948); L. M. Hartman, *ibid.* **73**, 316 (1948); H. Margenau, *ibid.* **73**, 326 (1948).
[40] J. M. Meek and J. D. Craggs, *Electrical Breakdown of Gases* (Clarendon, Oxford, 1953).
[41] S. C. Brown, *Introduction to Electrical Discharges in Gases* (Wiley, New York, 1966).
[42] J. M. Meek and J. D. Craggs, *Electrical Breakdown of Gases* (Wiley, Chichester, 1978).
[43] W. Schottky, Phys. Z. **25**, 635 (1929).
[44] L. Tonks and I. Langmuir, Phys. Rev. **34**, 876 (1929).
[45] A. von Engel, *Ionized Gases,* 2nd. ed. (Oxford Univeristy Press, Oxford, 1965).
[46] M. N. Hirsh and H. J. Oskam, *Gaseous Electronics 1:Electrical Discharges* (Academic, New York, 1978).
[47] A. von Engel, *Electric Plasmas: Their Nature and Uses* (Taylor & Francis, London, 1983).
[48] P. Bayle, J. Vacquie, and M. Bayle, Phys. Rev. A **34**, 360 (1986).
[49] T. J. Sommerer, W. N. G. Hitchon, and J. E. Lawler, Phys. Rev. A **39**, 6356 (1989).
[50] D. R. Nicholson, *Introduction to Plasma Theory* (Wiley, New York, 1983).
[51] M. J. Kushner, J. Appl. Phys. **54**, 4958 (1983).
[52] M. J. Kushner, IEEE Trans. Plasma Sci. **14**, 188 (1986).
[53] D. B. Graves and K. F. Jensen, Mater. Res. Soc. Symp. Proc. **68**, 219 (1986).
[54] M. S. Barnes, T. J. Colter, and M. E. Elta, J. Appl. Phys. **61**, 81 (1987).
[55] A. D. Richards, B. E. Thompson, and H. H. Sawin, Appl. Phys. Lett. **50**, 492 (1987).
[56] D. B. Graves J. Appl. Phys. **62**, 88 (1987).
[57] J. P. Boeuf, Phys. Rev. A **36**, 2782 (1987).
[58] R. W. Boswell and I. J. Morey, Appl. Phys. Lett. **52**, 21 (1988).
[59] B. E. Thompson and H. H. Sawin, J. Appl. Phys. **63**, 2241 (1988).
[60] K. Okazaki, T. Makabe, and Y. Yamaguchi, Appl. Phys. Lett. **54**, 1742 (1989).
[61] T. J. Sommerer, W. N. G. Hitchon, and J. E. Lawler, Phys. Rev. Lett. **63**, 2361 (1989).
[62] P. Belenguer and J. P. Boeuf, Phys. Rev. **41**, 4447 (1990).

[63] J. H. Tsai and C. Wu, Phys. Rev. A **41**, 5626 (1990).
[64] T. Makabe, F. Tochikubo, and M. Nishimura, Phys. Rev. A **42**, 3674 (1990).
[65] Y. H. Oh, N. H. Choi, and D. I. Choi, J. Appl. Phys. **67**, 3264 (1990).
[66] A. P. Paranjpe, J. P. McVittie, and S. A. Self, Phys. Rev. A **41**, 6949 (1990) and (unpublished).
[67] S. K. Park and D. J. Economou, J. Appl. Phys. **68**, 3904 (1990).
[68] M. Meyyappan and T. R. Govindan, IEEE Trans. Plasma Sci. **19**, 122 (1991).
[69] M. Surendra, D. B. Graves, and I. J. Morey, Appl. Phys. Lett. **56**, 1022 (1990).
[70] D. Vender and R. W. Boswell, IEEE Trans. Plasma Sci. **18**, 725 (1990).
[71] M. Surendra and D. B. Graves, IEEE Trans. Plasma Sci. **19**, 144 (1991).
[72] J. Wilhelm and R. Winkler, J. Phys. (Paris) Colloq. **40**, C7/251 (1979).
[73] T. J. Moratz, L. C. Pitchford, and J. N. Bardsley, J. Appl. Phys. **61**, 2146 (1987).
[74] R. Winkler and J. Wilhelm, in *Proceedings of the Nineteenth International Conference on Phenomena in Ionized Gases, Belgrade, Yugoslavia,* edited by V. J. Žigman (Faculty of Physics, University of Belgrade, Belgrade, 1989), invited papers pp. 108–117.
[75] N. Goto and T. Makabe, J. Phys. D **23**, 686 (1990).
[76] I. Yamanashi, N. Goto, and T. Makabe, Trans. IEE Jpn. **111-A**, 168 (1991).
[77] K. Kumar, H. R. Skullerud, and R. E. Robson, Aust. J. Phys. **33**, 343 (1980).
[78] I. P. Shkarofsky, T. W. Johnston, and M. P. Bachynski, *The Particle Kinetics of Plasmas* (Addison-Wesley, Reading, MA, 1966).
[79] J. M. Meek and J. D. Craggs, *Electrical Breaakdown of Gases* (Clarendon, Oxford, 1953).
[80] H. W. Ellis, R. Y. Pai, E. W. McDaniel, E.A. Mason, and L. A. Viehland, At. Data Nucl. Data Tables **17**, 177 (1976).
[81] G. Sejkora, P. Girstmair, H. C. Bryant, and T. D. Mark, Phys. Rev. A **29**, 3379 (1984).
[82] G. Dall'Armi, K. L. Brown, P. H. Purdie, and J. Fletcher (unpublished).
[83] C. W. Gear, *Numerical Initial Value Problems in Ordinary Differential Equations* (Prentice-Hall, Englewood Cliffs, NJ, 1971).
[84] C. A. M. de Vries, A. J. van Roosmalen, and G. C. C. Puylaert, J. Appl. Phys. **57**, 4386 (1985).
[85] R. A. Gottscho, Phys. Rev. A **36**, 2233 (1987).
[86] F. Tochikubo, T. Kokubo, A. Suzuki, S. Kakuta, Y. Terazono, and T. Makabe, in *Proceedings of the Twentieth International Conference on Phenomena in Ionized Gases, Pisa, Italy,* edited by V. Palleschi and M. Vaselli (Institute of Atom. Moelc. Phys.-CNR, Pisa, Italy, 1991), Vol. 5, pp. 1153–1154; F. Tochikubo, T. Makabe, S. Kakuta, and A. Suzuki, J. Appl. Phys (to be published).
[87] V. A. Godyak and A. S. Khanneh, IEEE. Trans. Plasma Sci. **PS-14**, 112 (1986).
[88] R. W. Crompton, M. Hayashi, D. E. Boyd, and T. Makabe, *Gaseous Electronics and Its Applications* (Kluwer Academic, Dordrecht, 1991).
[89] N. Mutsukura, K. Kobayashi, and Y. Machi, J. Appl. Phys. **66**, 4488 (1989).
[90] J. E. Velazco, J. H. Kolts, and D. W. Setser, J. Chem. Phys. **69**, 3457 (1978).
[91] R. S. Van Dyck Jr., C. E. Johnson, and H. A. Shugart, Phys. Rev. A **5**, 991 (1972).
[92] I. Yu. Baranov, V. I. Demidov, and N. B. Kolokolov, Opt. Spektrosk. **51**, 571 (1981) [Opt. Spectrosc. **51**, 316 (1981)].
[93] B. E. Cherrington, *Gaseous Electronics and Gas Lasers* (Pergamon, Oxford, 1979).
[94] F. Tochikubo and T. Makabe, Sci. Technol. **2**, 1133 (1991).
[95] P. Bletzinger, J. Appl. Phys. **67**, 130 (1990).
[96] K. Kohler, J. W. Coburn, D. E. Horne, E. Kay, and J. H. Keller, J. Appl. Phys. **57**, 59 (1985).